

A DNA Repair Inhibitor Isolated from an Ecuadorian Fungal Endophyte Exhibits Synthetic Lethality in PTEN-Deficient Glioblastoma

Nneoma Adaku,[#] Hyun Bong Park,[#] Daniel J. Spakowicz, Meetu Kaushik Tiwari, Scott A. Strobel, Jason M. Crawford,^{*} and Faye A. Rogers^{*}



Cite This: <https://dx.doi.org/10.1021/acs.jnatprod.0c00012>



Read Online

ACCESS |



Metrics & More



Article Recommendations



Supporting Information

ABSTRACT: Disruption of the tumor suppressor PTEN, either at the protein or genomic level, plays an important role in human cancer development. The high frequency of PTEN deficiency reported across several cancer subtypes positions therapeutic approaches that exploit PTEN loss-of-function with the ability to significantly impact the treatment strategies of a large patient population. Here, we report that an endophytic fungus isolated from a medicinal plant used by Indigenous Amazonians produces an inhibitor of DNA double-strand-break repair. Furthermore, the novel alkaloid product, which we have named irrepairzepine (1), demonstrated synthetic lethal targeting in PTEN-deficient glioblastoma cells. Our results uncover a new therapeutic lead for PTEN-deficient cancers and an important molecular tool toward enhancing the efficacy of current cancer treatments.



Glioblastoma multiforme (GBM) is the most common and aggressive form of primary cancer affecting the central nervous system in adults.¹ Among the most frequent genetic alterations implicated in the development of GBMs is loss of function mutations in the tumor suppressor PTEN, which are observed in 38% of these tumors.² PTEN (phosphatase and tensin homologue deleted on chromosome 10) is a negative regulator of the PI3K/AKT/mTOR signaling pathway and thus is involved in cellular proliferation, differentiation, and apoptosis.³ Mutated or deleted PTEN has been mechanistically associated with resistance to radiation and chemotherapy treatment in brain cancer patients.^{4,5} The current standard of care for GBM patients is surgical resection, followed by combination therapy with radiation and temozolomide.⁶ However, long-term success of this regimen remains poor, as almost all patients experience tumor progression with a median survival of less than 15 months.⁷ This dismal prognosis necessitates the discovery of new targeted approaches to add to the treatment paradigm. As a result, significant efforts have been made to apply inhibitors of the PTEN signaling pathway to the treatment of GBM, with little success in clinical trials to date.⁸

DNA repair pathways have long been recognized as critical players in the generation, treatment, and drug resistance of cancers, as DNA damage plays a dual role as both a creator of oncogenic mutations and a facilitator of cytotoxic genomic instability.⁹ Increasingly, the modulation of these pathways with small molecules is being explored as a therapeutic strategy, with the hallmark example being the FDA-approved

PARP inhibitor olaparib.¹⁰ By inhibiting the compensatory repair pathway that BRCA-deficient cancer cells rely upon for survival due to their dysfunctional homologous recombination-mediated double-strand-break (DSB) repair, PARP inhibitors are able to exploit a weakness conferred by the cancer-driving BRCA mutations. This targeted drug strategy based upon the genetic concept of synthetic lethality is expected to be selective for the DNA repair-deficient cancer cells with limited toxicity to normal tissues.¹¹ Moreover, nuclear PTEN has been implicated as a crucial factor in the maintenance of genomic stability since its loss is associated with chromosome aberrations and impaired DSB repair capacity.^{12–14} PTEN's role in numerous cellular processes, including the DNA damage response,^{15,16} positions its deficiency in cancer as a promising target for synthetic lethality treatment strategies. Indeed, multiple studies in different tumor types have explored the efficacy of existing inhibitors of PARP and the DNA damage signaling protein ATM in killing PTEN-deficient cancer cells, with promising results.^{16–20} However, the discovery of new, more efficacious DNA repair inhibitors is

Received: January 23, 2020



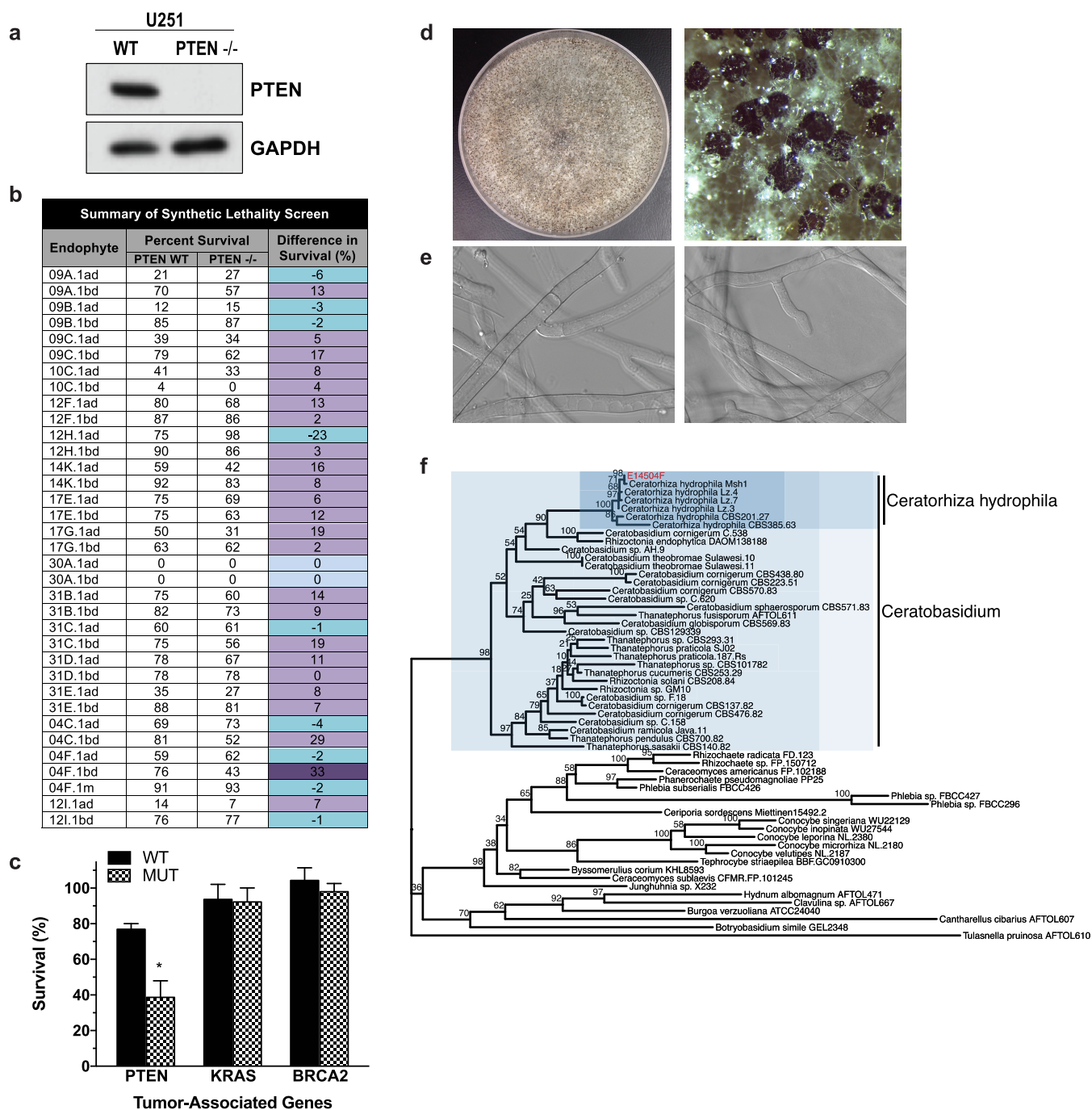


Figure 1. Identification of a bioactive endophyte extract. (a) Western blot analysis of PTEN expression in PTEN-deficient and -complemented U251 glioma cells. (b) Targeted crude endophytic extract screen in PTEN-proficient and -deficient U251 cells identifies a synthetic lethal interaction between PTEN-deficient cells and the E14504F (04F) extract. (c) Survival assays evaluating synthetic lethality interactions with other tumor-associated genes determine 04F activity is specific for PTEN deficiency. (d) Gross morphology of E14504F growth on PDA after 14 days at 27 °C. (e) Micromorphology on PDA. (f) Phylogenetic tree showing the relationship of E14504F to other fungi was constructed using the ITS, LSU, and RPB2 sequences. The fungal endophyte was identified as species *Ceratorhiza hydrophila*. The significant values are represented as * ($P < 0.05$).

an important next step in investigating this novel therapeutic approach to treating PTEN-deficient cancers.

Natural products have proven to be a reliable resource of new pharmaceutical agents. Over 50% of new medicines approved in the past four decades have been derived from or inspired by small molecules found in nature, and this number increases to over 60% for anticancer drugs.²¹ One especially promising natural source is metabolites produced by

endophytes. Endophytes are hyperdiverse microorganisms, primarily fungi and bacteria, that colonize the internal tissues of living plants without inflicting adverse effects.²² Many endophytes produce novel bioactive natural products that promote the survival of their host plants, but their potential for drug discovery still remains largely untapped.²³ In fact, only about 5% of the world's conservatively estimated 1.5 million fungal species have been described.²⁴ In some cases,

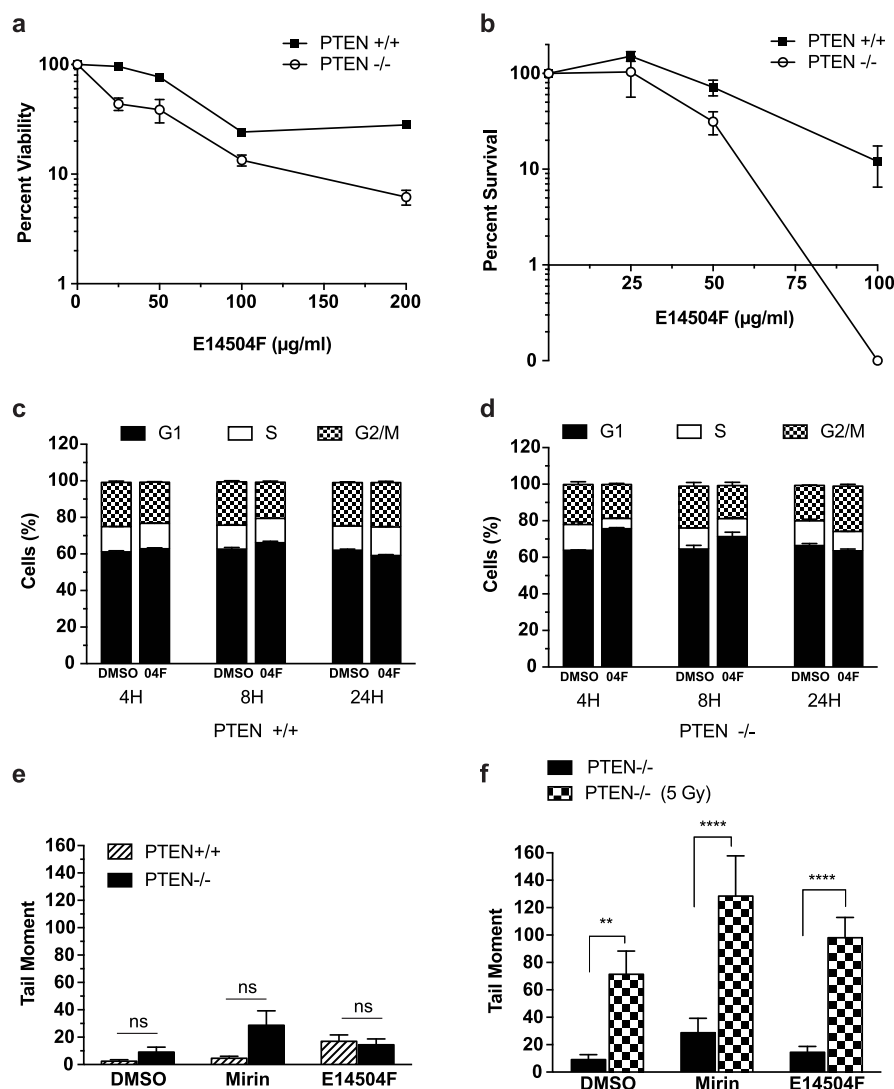


Figure 2. Evaluation of crude extract E14504F (O4F). (a) Evaluation of dose-dependent cell viability using the CellTiter-Glo luminescent assay 48 h post-treatment with O4F in PTEN-proficient and -deficient U251 cells. (b) Clonogenic survival assay in PTEN-proficient and -deficient U251 cells treated with the indicated doses of O4F. (c) Effect of O4F on cell cycle progression after treatment of U251 cells complemented with wild-type PTEN at various time points. (d) Effect of O4F on cell cycle progression in U251 PTEN-deficient cells. (e) Quantification of DNA strand breaks induced following O4F treatment using the neutral comet assay as measured by tail moment. (f) Neutral comet assay of PTEN-deficient cells with and without 5 Gy ionizing radiation (IR) in the presence of O4F. Statistical significance represented as asterisks: ** $P < 0.01$, **** $P < 0.0001$.

endophytes acquire the ability to synthesize natural products produced by their host plants.^{25,26} Perhaps the most notable example is the multibillion-dollar anticancer drug paclitaxel (Taxol). Paclitaxel was originally isolated from the Pacific yew tree,²⁷ a traditional medicinal plant used by Native Americans of the Pacific Northwest.^{28,29} However, additional studies later revealed that select endophytes from this plant could also produce the same compound.³⁰ This case provides support for an approach that utilizes traditional medicinal plants as a starting point to investigate endophytes for their production of biologically active compounds. Moreover, the use of fungal metabolites to achieve DSB repair inhibition also has precedence. Wortmannin, a compound isolated from the plant pathogen *Penicillium funiculosum*, is a known inhibitor of phosphoinositide 3-kinases such as DNA-PK.³¹ It has been shown to sensitize cells to radiation and chemotherapeutic drugs; however, its *in vivo* toxicity and instability make it unsuitable for clinical use.³²

Here, we describe the discovery of a novel DNA repair inhibitor produced by isolate E14504F of the endophytic fungus *Ceratorhiza hydrophila*, which was cultured from a sample of the medicinal plant *Pistia stratiotes* collected from the Pacific coast of Ecuador. This plant was sought out due to its reported use by the Ticuna people of the Northwest Amazon as a treatment for warts, a condition that, like cancer, is characterized by excessive cell proliferation.^{33,34} Activity-guided structural characterization demonstrated that the endophyte produces an azepine core-containing alkaloid, which we named irreparzepine (1), and that this novel molecule induces synthetic lethality in the genetic background of PTEN loss due to its demonstrated ability to inhibit DSB repair. Irreparzepine can potentially serve as an anticancer lead molecule for further development and treatment of PTEN-deficient GBMs.

RESULTS AND DISCUSSION

High-Throughput Screen Reveals a Fungal Extract with Synthetically Lethal Interactions in PTEN-Deficient Cells.

The forests of Ecuador have the greatest plant diversity in the world and therefore by extension perhaps possess great endophytic fungal and chemical diversity.³⁵ We collected plant samples from varied sites in Ecuador focusing our efforts toward medicinal plants that have been traditionally used by Indigenous populations to treat tumors or other diseases characterized by excessive cell proliferation. Eighty-four fungal endophytes were isolated from 24 different plant species collected across the country. Via internal transcribed spacer (ITS) sequencing and alignment with fungal sequences deposited in the NCBI's genetic sequence database GenBank, 17 of these endophytes were identified as potentially novel species and/or had limited mention in the literature, and thus were chosen for further investigation. We reasoned that the understudied nature of these organisms would increase the potential for identifying new compounds possessing our desired antineoplastic activity. We assembled a library of over 50 crude extracts derived from the 17 selected endophytes. Using a cell-viability-based high-throughput assay, we screened the endophytic crude extract library at a concentration of 50 $\mu\text{g}/\text{mL}$ to identify potential synthetic lethal interactions in cell line models with deficiencies commonly associated with cancer. PTEN protein expression levels in the U251 glioblastoma cell line and the isogenic PTEN-proficient cell line were validated by Western blot analysis (Figure 1a). Representative data from the primary screen in PTEN-deficient cells are shown in Figure 1b. A crude extract from fungal isolate E14504F demonstrated preferential cytotoxicity in PTEN-deficient glioblastoma cells compared to isogenic PTEN-proficient cells with a 33% difference in survival, suggesting that the endophyte produced a compound that is active in the cellular landscape formed by PTEN loss (Figure 1b). This specificity was confirmed by the lack of activity in cell lines mutated in the tumor-associated genes, KRAS and BRCA2 (Figure 1c). Phylogenetic and morphogenic analysis identified the fungal endophyte as species *Ceratorhiza hydrophila* (Figure 1d–f, Figures S1–S3 and Table S1).

Evaluation of Crude Extract E14504F Bioactivity.

Crude extract E14504F (04F) was further evaluated for its potency against PTEN-deficient glioma cells. Using our cell viability assay, 04F demonstrated dose-dependent cytotoxicity in U251 cells, with synthetic lethality in PTEN-deficient cells persisting across all tested doses (Figure 2a). This activity was confirmed via a clonogenic survival assay, where the effect was even more pronounced, as there were no viable PTEN-deficient colonies at the 100 $\mu\text{g}/\text{mL}$ dose of the crude extract (Figure 2b). Next, we investigated the impact of 04F treatment on cell cycle progression at multiple time points. Notably, substantial G1 arrest in the PTEN-deficient cells was observed 4 h post-treatment with the crude extract, while no effect was seen in the PTEN-proficient cell population (Figure 2c,d). One of the most powerful activators of the G1/S checkpoint is DNA damage, as this checkpoint works to prevent damaged DNA from being replicated during the S phase.³⁶ We sought to assess this potential mechanism of action by evaluating repair capacity in the presence of the crude 04F extract. We used the neutral comet assay to evaluate the presence of DSBs after ionizing radiation (IR), which is a commonly used approach to

measure functional DSB repair activity. It is important to note that no significant damage was detected above background following simple addition of the crude extract (Figure 2e). However, we detected a reduced capacity for DSB repair following IR exposure (5 Gy) in PTEN-deficient cells pretreated with 04F crude extract (Figure 2f). Similar increased persistence of unrepaired DSBs was also observed with cells treated with the DSB repair inhibitor mirin, which targets the Mre11-Rad50-Nbs1 (MRN) complex, a key DNA damage sensor for homology-directed repair of DSBs.

Structure Elucidation of Compound 1. To elucidate the structure of the DNA repair inhibitory metabolite present in the crude extract, a 6 L culture of E14504F was initiated. After cultivation for 2–3 weeks at 27 °C, the whole culture broth was extracted with 12 L of methylene chloride and fractionated using reversed-phase HPLC systems for bioassay-guided identification (see Endophyte Isolation, Experimental Section, and Figures S4 and S5). Three sequential rounds of HPLC purification and activity analysis yielded active compound 1 ($t_{\text{R}} = 20.9$ min, 0.2 mg), (Figure S6), which was characterized by mass spectrometry (MS), UV (Figures S7 and S8), and NMR (Figure 3). Compound 1 was isolated as an amorphous solid

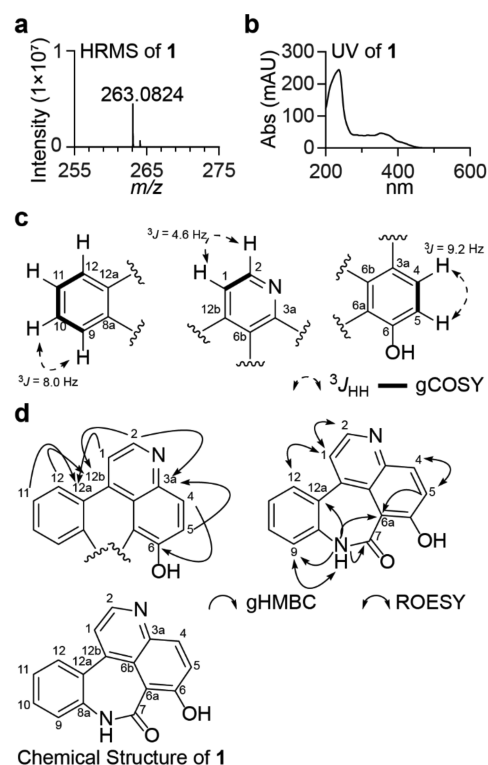


Figure 3. Structure elucidation of irreparzequine (1). (a) High-resolution ESI-QTOF-MS spectrum of 1. (b) UV–visible spectrum of 1. (c) ^1H coupling constants and ^1H – ^1H gCOSY correlations of 1 in $\text{DMSO}-d_6$. (d) Key gHMBC and ROESY correlations of 1 in $\text{DMSO}-d_6$.

with a molecular formula of $\text{C}_{16}\text{H}_{10}\text{N}_2\text{O}_2$ based on its high-resolution electrospray ionization–quadrupole time-of-flight–mass spectrometry (HR-ESI-QTOF-MS) spectrum (Figure 3a). The UV–visible spectrum of compound 1 revealed absorption maxima at 242 and 360 nm (Figure 3b).³⁷

The chemical structure of 1 was characterized based on the interpretation of its ^1H and 2D (gCOSY, gHSQC, gH2BC, gHMBC, and ROESY) NMR spectra (Table 1 and Figures

Table 1. NMR Data of 1

no.	DMSO- <i>d</i> ₆				MeOH- <i>d</i> ₄		
	δ_C^a	type	δ_H^b	mult (<i>J</i> in Hz)	δ_C^a	δ_H^b	mult (<i>J</i> in Hz)
1	122.9	CH	7.65	d (4.6)	122.3	7.81	d (5.1)
2	148.3	CH	8.72	d (4.6)	144.9	8.73	d (5.1)
3		N					
3a	143.3	C	139.8				
4	137.8	CH	8.08	d (9.2)	133.4	8.11	d (9.3)
5	124.2	CH	7.40	d (9.2)	125.5	7.53	d (9.3)
6	166.2	C	166.7				
6a	106.4	C	106.2				
6b	128.7	C	129.2				
7	175.6	C					
8		NH	10.48	br s			
8a	137.6	C	137.6				
9	121.2	CH	7.28	d (7.8)	120.3	7.20	dd (8.5, 1.2)
10	131.2	CH	7.43	t (7.8)	131.3	7.48	m ^c
11	126.1	CH	7.24	t (7.8)	125.6	7.29	dt (7.5, 1.2)
12	132.6	CH	7.41	m ^c	132.3	7.48	m ^c
12a	127.9	C	126.9				
12b	142.0	C	146.2				
OH			6.51	br s			

^aAssigned by HSQC and HMBC. ^b600 MHz. ^cOverlapping signals.

S9–S23). First, a ¹H NMR spectrum in MeOH-*d*₄ (Figures S9 and S10) displayed the resonances of eight well-resolved aromatic protons (δ_H 8.73–7.20). Sequential COSY correlations (Figure S11) from aromatic proton H9 (δ_H 7.20, dd, *J* = 8.5, 1.2 Hz) to proton H12 (δ_H 7.48, m, overlapping signal) supported a 1,2-disubstituted benzene ring (Figure S11). The ¹H–¹H coupling constant (5.1 Hz) coupled with a strong COSY cross-peak between doublet protons H1 (δ_H 7.81) and H2 (δ_H 8.73) that is often observed in nitrogen-containing aromatic systems also suggested the presence of a pyridine moiety (Figure S11).³⁸ Additionally, a coupled H4 (δ_H 8.11, d, *J* = 9.3 Hz) and H5 (δ_H 7.53, d, *J* = 9.3 Hz) deduced a tetrasubstituted aromatic ring constituted by a hydroxy group (Figure S11 and Table 1).³⁹ The gHSQC and gH2BC NMR spectra of 1 also allowed us to assign all these protons to bonded sp² carbons at δ 144.9 (C2), 133.4 (C4), 122.3 (C1), 125.5 (C5), 131.3 (C10), 132.3 (C12), 125.6 (C11), and 120.3 (C9) (Figures S12 and S13). The connectivity of these three-ring systems was established by HMBC spectroscopy (Figure 3 and Figures S14 and S15). Two long-range HMBC correlations sharing nonprotonated carbon C3a (δ_C 139.8) from H2 and H5 and nonprotonated carbon C6b (δ_C 129.2) from H4 and H1 supported a quinoline-type moiety. An additional three-bond HMBC correlation from H4 to downfield shifted carbon C6 (δ_C 166.7) further suggested that this moiety is substituted with a hydroxy group at C6.³⁹ HMBC correlations from H11 and H1 to C12a (δ_C 126.9) and from H12 and H2 to C12b (δ_C 146.2) elucidated the connectivity of these two rings via a C–C bond (Figures S14 and S15). In addition, H10 and H5 had three-bond HMBC correlations with the two nonprotonated carbons C8a (δ_C 137.6) and C6a (δ_C 106.2). Lastly, the chemical formula deduced from the high-resolution MS data allowed us to suggest the presence of an amino carbonyl group bound to C8a and C6a, establishing a fourth ring.

Additional NMR spectra in aprotic DMSO-*d*₆ (Figure 3c,d, Table 1, and Figures S16–S23) supported the expected exchangeable protons 8-NH (δ_H 10.48, br s) and 6-OH (δ_H 6.51, br s) (Figures S16 and S17). The ¹H and ¹³C chemical shifts in DMSO (Table 1) were nearly identical to those of NMR spectra recorded in MeOH (Table 1). However, the observation of an additional carbon C7 (δ_C 175.6) strongly supported the presence of the previously proposed amide carbonyl group, and the key gHMBC correlations from proton 8-NH to C7, C9, C6a, and C12a unambiguously determined the full structure of compound 1 (Figure 3d and Figure S20). 2D ROESY experiments also supported the structure based on ROESY cross-peaks between H1 and H12, 8-NH, and H9 (Figure 3d and Figures S21–S23). Thus, the full chemical structure of 1 was determined to be a new endophytic fungal alkaloid, 2-hydroxybenzo[6,7]azepino[5,4,3-*de*]quinolin-4(5*H*)-one, termed irreparzepine (1).

A 5-aminobenzoazepinoquinolinone (ABAQ) analogue of irreparzepine has previously been synthesized by the non-enzymatic Maillard reaction.³⁷ To determine whether this reaction could produce irreparzepine, we conducted an identical Maillard reaction with the two substrates D-glucose and L-tryptophan, following the literature protocol. While ABAQ was detected as expected, irreparzepine (1) was not detected in our experiments (Figure 4). Interestingly, β -carboline and ABAQ were detected in both the fungal extract

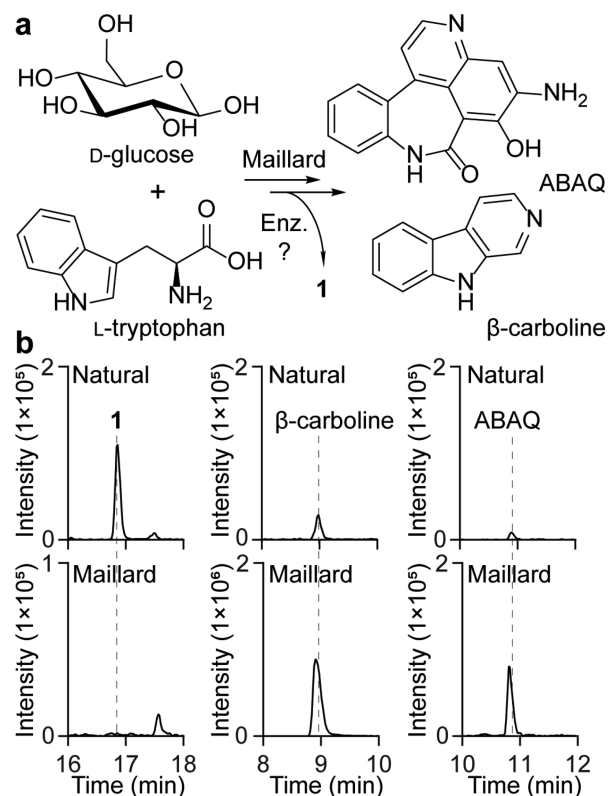


Figure 4. Proposed biosynthesis route of irreparzepine via a Maillard-type pathway. (a) Products from an *in vitro* Maillard chemical reaction with D-glucose and L-tryptophan. The fungus produces the Maillard products β -carboline and ABAQ, and 1 is likely derived from an uncharacterized Maillard-type biosynthetic pathway. (b) Extracted ion count chromatograms corresponding to 1 (*m/z* 263.0821), β -carboline (*m/z* 169.0766), and ABAQ (*m/z* 278.0930) from the natural fungal extract and the Maillard chemical reaction.

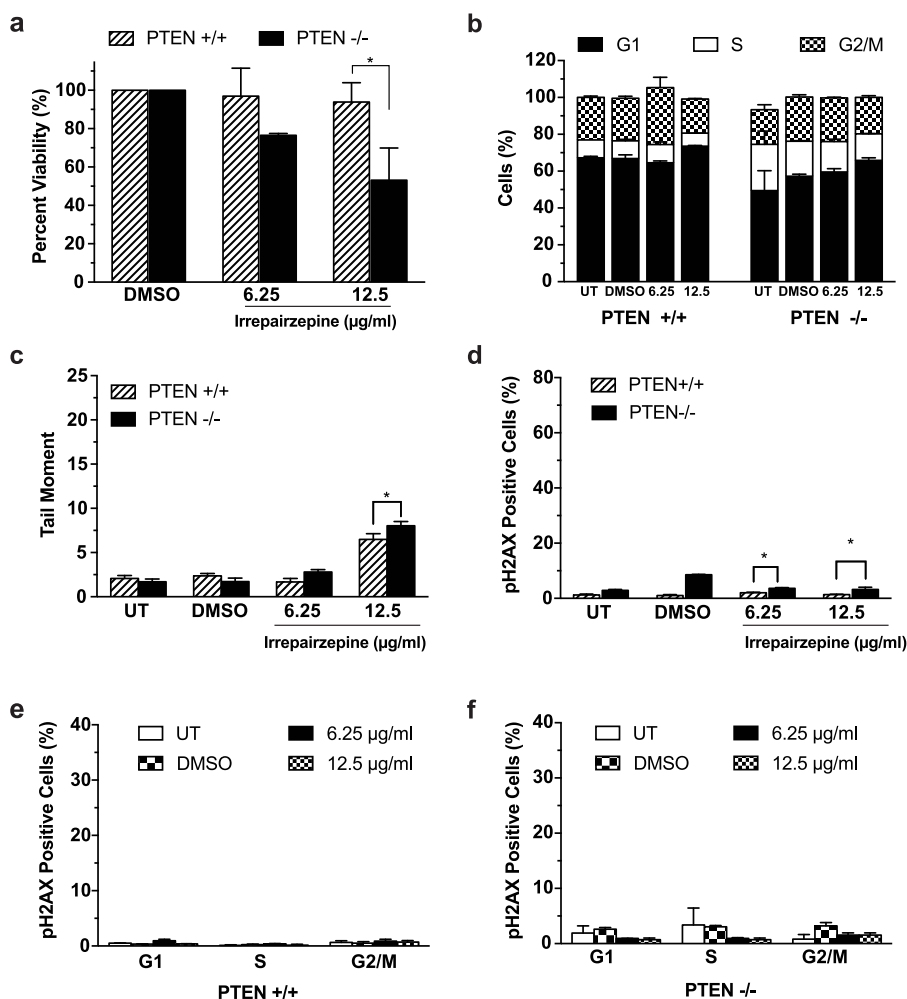


Figure 5. Irreparzepine is synthetic lethal in PTEN-deficient cancers. (a) Effect of irreparzepine on the cell viability of PTEN-proficient and -deficient cells. (b) Effect of irreparzepine on cell cycle progression. (c) Effect of irreparzepine on the repair of endogenous DSBs as determined by the neutral comet assay. (d) Determination of γ H2AX-positive cells as a measure of DNA damage. (e) Measure of γ H2AX-positive cells at various stages of the cycle in PTEN +/+ cells. (f) Identification of PTEN -/- cells positive for DNA damage at various phases of the cell cycle following irreparzepine treatment. Statistical significance indicated as * ($P < 0.05$). UT indicates untreated.

and the Maillard reactions (Figures S24 and S25). Consequently, a novel and currently uncharacterized Maillard-type pathway in the fungus is likely responsible for irreparzepine biosynthesis.

Irreparzepine Mediates E14504F Synthetic Lethal Interactions with PTEN Deficiency. We then proceeded to confirm irreparzepine's contribution to its parental crude extract E14504F's bioactivity. The purified molecule irreparzepine recapitulated 04F's selective cytotoxic activity against PTEN-deficient U251 cells (Figure 5a). Similar to the crude extract, addition of irreparzepine resulted in a slight increase in the proportion of cells in the G1 phase, suggesting activation of the G1/S DNA damage checkpoint (Figure 5b). The neutral comet assay was again utilized to interrogate irreparzepine's impact on DSB repair. Additionally, DNA damage that results in DSBs is followed by the phosphorylation of histone H2AX on serine 139. As a result, this phosphorylated form of H2AX, also referred to as γ H2AX, is often used as a biomarker of DNA DSBs. Treatment with irreparzepine alone was sufficient to induce significantly more DNA damage in the PTEN-deficient cells compared to PTEN-proficient, suggesting possible inhibition of the repair of naturally occurring DSBs

(Figure 5c,d). However, this increase in DSBs did not appear to be cell cycle dependent (Figure 5e,f).

Irreparzepine Inhibits DSB Repair. Next, we investigated the mechanism by which irreparzepine can induce a synthetic lethal effect in a PTEN-deficient genetic background. As discussed above, PTEN loss is associated with impaired DSB repair, and crude extract 04F was capable of enhancing IR-mediated DNA damage in the PTEN-deficient context. Thus, we tested whether irreparzepine could inhibit DSB repair using an established chromosomally integrated fluorescent NHEJ/HR dual-reporter in U2OS cells (U2OS EJ-DR cells).⁴⁰ The dual repair system is based on site-specific DSBs induced by the rare-cutting endonuclease I-Sce-I.⁴¹ The direct repeat GFP (DR-GFP) is a commonly used HR reporter, and the NHEJ assay will measure any mutagenic NHEJ (mNHEJ) repair events, such as insertions and deletions, following creation of the DSB by I-Sce-I. To evaluate irreparzepine's capacity to inhibit DSB repair, U2OS EJ-DR cells were incubated with irreparzepine and a DSB inducer for 24 h and analyzed 96 h later by flow cytometry. A reduction in HR (46%) and mNHEJ (48%) activities was observed at a dose of 12.5 μ g/mL (Figure 6a,b). These results suggest that irreparzepine selectively represses DSB repair.

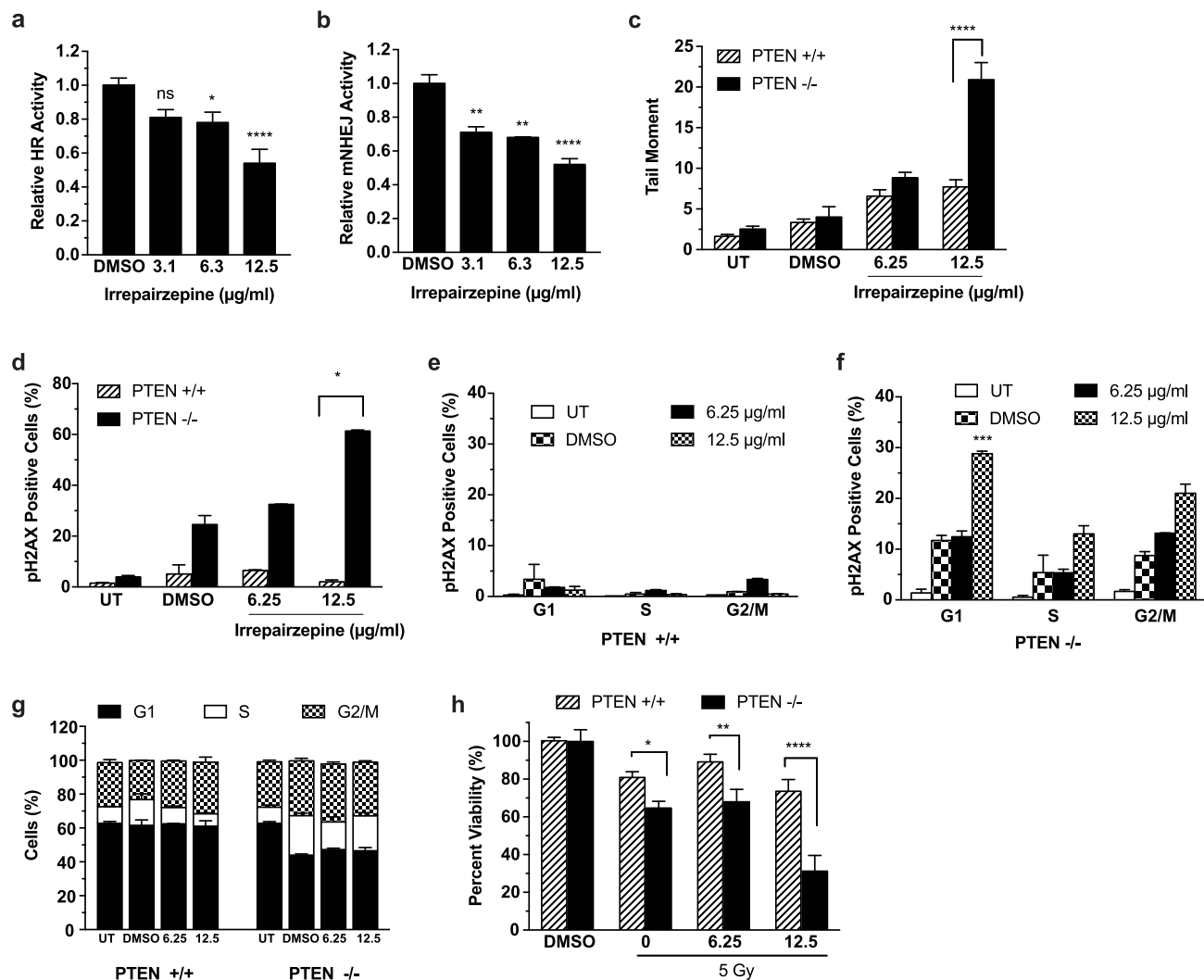


Figure 6. Irreparzepine inhibits DSB repair. (a) Effect of irreparzepine on HR activity in U2OS EJ-DR cells. (b) Effect of irreparzepine on mNHEJ in U2OS EJ-DR cells. (c) Neutral comet assay after IR treatment (5 Gy). (d) Level of IR-induced DNA damage in the presence of irreparzepine as measured by γ H2AX positivity. (e) Evaluation of γ H2AX-positive PTEN-proficient cells after IR treatment in various phases of the cell cycle. (f) Cell cycle analysis of γ H2AX-positive PTEN-deficient cells after IR treatment at various concentrations of irreparzepine. (g) Evaluation of irreparzepine pretreatment on cell cycle progression following 5 Gy IR treatment. (h) Evaluation of irreparzepine as a potential radiosensitizer as determined by the CellTiter-Glo cell viability assay. Statistical significance represented as asterisks: * $P < 0.05$, ** $P < 0.01$, *** $P < 0.001$, and **** $P < 0.0001$. UT indicates untreated.

We then used the neutral comet assay to measure the persistence of DSBs after IR treatment. We detected a significant reduction in the capacity to repair IR-induced DSBs after irreparzepine pretreatment as indicated by an increase in comet tail moments in the PTEN-deficient cells at a dose of 12.5 μ g/mL (Figure 6c). Analysis of γ H2AX resolution after combined irreparzepine and IR treatment also confirmed our comet assay results, as we observed a delay in repair activity (Figure 6d). The formation of γ H2AX foci in cells after irradiation is a very sensitive assay for DSB measurement. As would be expected, the majority of the γ H2AX-positive PTEN-deficient cells were found in the G1 phase of the cell cycle (Figure 6e,f).

We then proceeded to investigate whether irreparzepine had the capacity to enhance the effectiveness of currently used anticancer therapies. Drugs that inhibit the functional DSB repair pathways in the repair-deficient tumor cells can also potentiate the activity of DNA-damaging agents. Normal cells, which are less reliant on the compensatory pathways, are not

sensitized by the repair inhibitor to the same degree, resulting in potentially less toxicity to normal tissue. Hence, concurrent administration of DSB repair inhibitors and DNA-damaging agents can enhance tumor control. Since radiation therapy is the current standard of care for many cancers, including GBM, we proceeded to investigate the potential for irreparzepine to serve as a radiosensitizer. Although efficient DNA repair has been correlated with G2 arrest and radioresistance,⁴² other studies have reported that radiosensitization induced by PARP inhibition is accompanied by elongation of G2/M arrest.⁴³ We pretreated PTEN-deficient and PTEN-proficient U251 cells with irreparzepine for 4 h followed by treatment with IR (5 Gy). Cell cycle analysis revealed an increase in the level of cells in the G2/M phase (Figure 6g). Additionally, cell viability was assessed using CellTiter-Glo after combination treatment with irreparzepine and a single dose of 5 Gy. Treatment with irreparzepine enhanced the irradiation cytotoxic effects with a decrease in cell survival observed in the PTEN-deficient cells compared to treatment with IR alone (Figure 6h). These

results suggest that irreparzepine can be used in combination with DNA-damage-based therapies to enhance their efficacy.

The cancer field has recently seen a substantial increase in the number of FDA-approved therapies compared to previous decades, and this has been accompanied by a shift toward drugging cancer-specific molecular pathways rather than a broad cytotoxic approach.⁴⁴ However, this rapid progress has not yet reached GBM, whose only unique treatment is the nonspecific alkylating agent temozolomide, which achieved FDA approval 20 years ago. Irreparzepine's ability to substantially kill PTEN-deficient glioma cells on its own, in addition to sensitizing these cells to IR-induced DNA damage, makes it a potentially attractive candidate for combination with radiation therapy. Moreover, as PTEN loss is a common genomic alteration in multiple cancers including melanoma, prostate, uterine, and lung,⁴⁵ irreparzepine could potentially serve as a therapeutic lead for tumors beyond GBM. Given irreparzepine's ability to inhibit both HR and mNHEJ in the U2OS EJ-DR assay, it potentially interacts with a protein at the interface of these two distinct repair pathways. Future identification of irreparzepine's biological target may add to our current understanding of PTEN's role in the DNA damage response and the genomic consequences of its loss. Furthermore, irreparzepine can serve as a lead scaffold in medicinal chemistry efforts to design more potent DSB repair inhibitors with improved drug efficacy in PTEN-deficient cancers. Taken together, our work emphasizes the power in combining endophytic diversity and natural product research methods with new molecular pathway targeting approaches as a strategy for novel anticancer drug discovery.

■ EXPERIMENTAL SECTION

General Experimental Procedures. ¹H and 2D (gCOSY, gHSQC, gHMBC, gH2BC, and ROESY) NMR spectra were recorded on an Agilent 600 MHz NMR spectrometer equipped with a cold probe (Agilent, Santa Clara, CA, USA). HPLC isolation was performed over an Agilent Prepstar HPLC system with a Phenomenex Luna C₁₈(2) (100 Å) 10 μm (10.0 × 250 mm) column (Phenomenex, Torrance, CA, USA) and an Agilent Phenyl-Hexyl 5 μm (9.4 × 250 mm) column. HPLC/MS analysis was performed on an Agilent 1260 Infinity Quaternary LC system consisting of an autosampler, a quaternary solvent delivery system, a thermostat-controlled column compartment, and a diode-array detector (DAD) coupled to an Agilent 6120 Quadrupole low-resolution (LR) electrospray ionization (ESI) mass spectrometer. High-resolution (HR) ESIMS data was obtained using an Agilent iFunnel 6550 QTOF (quadrupole time-of-flight) MS instrument fitted with an ESI source coupled to an Agilent 1290 Infinity HPLC system.

Endophyte Isolation. Clumps of the free-floating aquatic medicinal herb *Pistia stratiotes* (Araceae) were found growing in a stream near Same Beach on the Pacific coast of Ecuador (0.84851 S, 79.92265 W). The root and leaves of a single plant were collected, rinsed of dirt, placed into an airtight plastic bag, and stored at 4 °C until processing 13 days later. The specimens were externally sterilized by a 5 s submersion in 70% ethanol followed by a brief flaming. The external plant tissues were then removed via scalpel, and the internal tissues were exposed on plates containing water agar (15 g agar/L), 0.1× potato dextrose agar (PDA; 2.4 g of EMD Millipore potato dextrose/L), or a 0.1× malt extract agar (MEA), and the plates were monitored every 1–2 days for endophyte outgrowth. *C. hydrophila* E14504F was identified on the 0.1× MEA plate 6 days after plating and was transferred to a 0.1× PDA plate to obtain a pure culture. The isolated fungus was then cultured on 1× PDA plates, and permanent stocks of the fungus were formed by placing 1× PDA plugs of fresh mycelium into freezer tubes filled with sterile distilled water and storing them at room temperature. Other medicinal plants were

similarly collected throughout Ecuador and processed to isolate several endophytes that contributed to the formation of a crude extract library.

Generation of the Crude Extract Library. To determine the identities of isolated endophytes, fungal DNA was sequenced at the ITS region, which is considered the universal barcode sequence for fungi, and compared to known fungal sequences hosted in the NIH genetic sequence database GenBank. Fungi with ≤95% sequence homology were hypothesized to be potentially novel organisms and were chosen for organic extraction. PDA plugs (5 mm, 1× PDA) inoculated with the desired endophyte were added to culture tubes containing 5 mL of autoclaved potato dextrose broth (PDB) and incubated at room temperature for 7 days. The liquid culture was then expanded to a culture flask containing sterile PDB (100 mL) and incubated for an additional 7–8 days at room temperature. Cultures were then expanded to 1 L, and the fungi were allowed to grow for 2 weeks stationary at room temperature or shaking at 30 °C to enrich for secondary metabolite production. The contents of each flask were filtered through cheesecloth, and the isolated mycelial mass was soaked in methanol (100 mL) overnight to form a cellular crude extract. The filtered PDB was extracted at pH 5.5 and pH 9 using dichloromethane (800 mL). The resulting three crude extracts from each endophyte are identified as methanol (0.1m), acidic (0.1ad), and basic (0.1bd).

DNA Isolation and Sequencing. *C. hydrophila* E14504F was grown in potato dextrose broth for 14 days, after which the mycelium was harvested and the genomic DNA purified using a DNeasy plant mini kit (Qiagen; Hilden, Germany) according to the manufacturer's protocols. The ITS, LSU, and RPB2 loci were amplified using GoTaq Flexi (Promega; Madison, WI, USA) and standard primers (Table S1). Amplicons were sequenced at the W.M. Keck Facility at Yale University in forward and reverse directions. Consensus sequences were generated and manually curated for consistency using the Staden package v2.0.0b8⁴⁶ and were deposited in GenBank (accession numbers: MT381951–MT381956).

Database Comparisons. DNA sequences were classified by comparison to several curated online databases, recently reviewed by Prakash et al.⁴⁷ Searching the LSU sequence against the SILVA database returned no taxonomic assignments above confidence threshold. Searching the LSU sequence against the Ribosomal Database Project returned 100% confidence in the genus *Thanatephorus*, within the family Ceratobasidiaceae, order Cantharellales. This genus had been recently circumscribed by Gonzalez et al. in an effort to clarify the Rhizoctonia, an anamorphic genus found to be polyphyletic by molecular methods.⁴⁸ The BOLD Systems database search of the ITS sequence returned 92% similarity to *Sclerotium hydrophilum*, in the order Agaricales. The UNITE database ITS search resulted in equiprobable matches to *Thanatephorus cucumeris* as well as another genus in the Ceratobasidiaceae, *Ceratohiza hydrophila*. To clarify the discrepancy between these databases, representatives from each of the clades were retrieved for multilocus phylogenetic analysis.

Phylogenetic Analysis. A phylogenetic tree showing the relationship of E14504F to other fungi was constructed using ITS, large ribosomal subunit (LSU), and RNA polymerase II (RPB2) sequences (Table S3). Comparison sequences were included if voucher specimens of the organism are available in public repositories and the sequence is associated with a publication. Sequences were aligned using the muscle implementation within the APE package v4.1⁴⁹ using R v3.4.2⁵⁰ in RStudio v1.1.383.⁵¹ Gaps in more than 30% of the alignments were removed. Optimal substitution models were identified for each alignment using the modelTest implementation in the Phangorn package v2.2.0.⁵² For each locus, a neighbor-joining tree was optimized by the maximum likelihood method using a GTR+G model, and then 100 bootstrap replicates were performed. The loci were then interleaved and a tree was constructed using RAXML v8.2.10⁵³ and visualized using ggtree v1.8.2.⁵⁴ All code for generating the trees, including retrieving comparison sequences, is available at <https://github.com/dspak/e14504f>.

Organic Extraction and Bioactivity-Guided Isolation of Irreparzepine. A 6 L stationary fungal culture was filtered through

cheesecloth, and the culture broth was extracted with 12 L of methylene chloride (MC) (2 × 6 L) followed by rotary evaporation to remove organic solvent and yield approximately 100 mg of dried MC-soluble fraction. The crude materials were tested for synthetic lethality in PTEN-deficient cell lines and analyzed on an Agilent single quadrupole LC/MS system (column, Phenomenex Kinetex C18 (100 Å) 5 μm (4.6 × 250) mm; flow rate, 0.7 mL/min; mobile phase composition, water–acetonitrile (ACN) gradient system containing 0.1% formic acid (v/v): 0–30 min, 10–100% ACN; hold for 5 min, 100% ACN; 2 min, 100–10% ACN; 5 min post-time, 10% ACN). The active crude materials were subsequently resuspended in the initial mobile phase, and methanol was added dropwise to completely dissolve the materials. Twelve time-dependent HPLC fractions were manually collected through the reversed-phase C₁₈ column [(100 Å) 10 μm (10.0 × 250 mm)] with the following separation conditions: (flow rate, 4 mL/min; mobile phase composition, water–ACN gradient system containing 0.1% formic acid (v/v): 10 min, 10% ACN in water; 60 min, 10–100% ACN). Each of the 12 fractions was tested, and partially pure fraction 10 (1.5 mg) was active in the bioassay. Fraction 10 was further purified using an isocratic method (40% ACN over 30 min, 4 mL/min) through the same C₁₈ column and then over an Agilent Phenyl-Hexyl 5 μm (9.4 × 250) mm column eluting with a gradient separation (10–100% ACN in water over 60 min; 4 mL/min) to yield pure compound 1 (*t*_R = 20.9 min, 0.2 mg).

Irrepairzepine (1): amorphous solid; NMR spectra, see Table 1; HR-ESI-QTOF-MS [M + H]⁺ *m/z* 263.0824 (calcd for C₁₆H₁₁N₂O₂, 263.0821).

Cell Culture. U251 cells were cultured in DMEM supplemented with 10% FBS, while their PTEN-inducible counterparts (U251-PTEN⁵⁵) were cultured in DMEM with 10% FBS, 400 μg/mL G418, 2 μg/mL blasticidin, and 1 μg/mL doxycycline to activate PTEN expression. PEO1 and PEO1 C4-2 cells (BRCA2-deficient and -proficient, respectively) were cultured in RPMI supplemented with 10% FBS, and CAL-12T cells and their KRAS mutant counterparts were cultured in DMEM with 10% FBS. U2OS EJ-DR cells were cultured in DMEM supplemented with 10% tetracycline (TET)-free FBS. All cell lines were maintained at 37 °C with 5% CO₂.

Synthetic Lethality Screen. The CellTiter-Glo luminescent cell viability assay (Promega) was utilized as an initial high-throughput screen for synthetic lethality. Cells were seeded into white-bottomed 96-well plates at a density of 2500–5000 cells/well 24 h prior to treatment. Compounds were dissolved in DMSO and added at the respective concentrations, and 48 h later 50 μL of CellTiter-Glo reagent was added per well after the plate and reagent were equilibrated to room temperature. Plates were shaken for 2 min to induce cell lysis and then spun down at 1000 rpm for 1 min. After a 30 min incubation at room temperature, luminescence was measured with a BioTek Synergy HT microplate reader.

U2OS EJ-DR Reporter Assay. Log-phase U2OS EJ-DR cells were seeded into 96-well plates at a density of 1 × 10⁴ cells/well. To induce endonuclease-mediated DNA cleavage, TET-free media was supplemented with the ligands Shield1 and triamcinolone acetonide (TA) at respective concentrations of 0.5 and 1 μmol/L. Irrepairzepine was dissolved in DMSO and added to wells in triplicate. After 24 h, cells were washed with 1× PBS and were then split into two wells with 0.05% trypsin to prevent overconfluence. After another 72 h of incubation in fresh TET-free media, the two wells were recombined and transferred to tubes for FACS analysis with the BD FACSCalibur platform. HR and mNHEJ activity were evaluated by quantifying the number of GFP-positive and DsRed-positive cells, respectively, with an acquisition number of 1000–2500 cells/well. Repair activity was normalized to that of cells treated with 1% DMSO.

Clonogenic Survival Assay. Cell lines were plated in triplicate 24 h prior to treatment at a density of 200–400 cells/well in 12-well plates. Cells were then treated with crude extract for 48 h, and culture media was replaced every 2 days until colonies formed. Cells were then stained with crystal violet in 80% methanol, and colonies were quantified.

Neutral Comet Assay. Cells were seeded at a density of 10 000 cells/well into a 96-well plate 24 h prior to treatment. On the day of

treatment, DMSO, 04F (50 μg/mL), or mirin (positive control; 25 μM) was added to the cells 8 or 24 h prior to their collection. Irrepairzepine was added at 6.25 or 12.5 μg/mL. For irradiated cells, irradiation was performed at a dose of 5 Gy 4 h after the addition of extract. The assay was performed per the manufacturer's (Trevigen) instructions, and comets were visualized on an Axiovert 200 microscope at 10× magnification and 40% intensity. Approximately 50 comets were analyzed per treatment condition with Cometscore software, and mean tail moment was calculated.

Cell Cycle Analysis and γH2AX. Cells were collected at 4, 8, and 24 h following treatment with 04F or irrepairzepine with and without IR treatment. After washing once with PBS, the cells were fixed in 1% paraformaldehyde for 15 min on ice. Cells were centrifuged and fixed in 70% ethanol at –20 °C for 2 h. The cells were then washed with BSA-T-PBS (1% w/v bovine serum albumin and 0.2% v/v Triton X-100 in PBS) and incubated with γH2AX antibody (Cell Signaling) in BSA-T-PBS overnight at 4 °C. After washing, the cells were incubated with anti-rabbit IgG Fab2 Alexa 488 (Molecular Probes) at room temperature for 1 h in the dark. Cells were washed, and the pellet was resuspended and incubated at room temperature in PI staining solution (PI/PNase solution, BD) for 15 min. Cells were analyzed by flow cytometry.

Statistical Analysis. Statistical analysis was performed by one-way or two-way ANOVA with the Tukey's *post hoc* test. All analysis was completed using GraphPad Prism software. *****P* < 0.0001, ****P* < 0.001, ***P* < 0.01, **P* < 0.05.

■ ASSOCIATED CONTENT

Supporting Information

The Supporting Information is available free of charge at <https://pubs.acs.org/doi/10.1021/acs.jnatprod.0c00012>.

Phylogenetic tree of the fungal strain (E14504F), HPLC/MS analysis, activity-guided fractionation, and HR-ESI-Q-TOF-MS, UV, and NMR spectra of compound 1 (PDF)

■ AUTHOR INFORMATION

Corresponding Authors

Jason M. Crawford – Department of Chemistry and Chemical Biology Institute, Yale University, New Haven, Connecticut 06520, United States; Department of Microbial Pathogenesis, Yale School of Medicine, New Haven, Connecticut 06536, United States; orcid.org/0000-0002-7583-1242; Phone: (203) 737-3966; Email: jason.crawford@yale.edu

Faye A. Rogers – Department of Therapeutic Radiology and Yale Cancer Center, Yale School of Medicine, New Haven, Connecticut 06520, United States; orcid.org/0000-0002-1454-9892; Phone: (203) 737-3658; Email: faye.rogers@yale.edu

Authors

Nneoma Adaku – Department of Therapeutic Radiology, Yale School of Medicine, New Haven, Connecticut 06520, United States; orcid.org/0000-0001-9287-6744

Hyun Bong Park – Department of Chemistry and Chemical Biology Institute, Yale University, New Haven, Connecticut 06520, United States; orcid.org/0000-0002-2986-3833

Daniel J. Spakowicz – Department of Molecular Biophysics and Biochemistry, Yale University, New Haven, Connecticut 06520, United States

Meetu Kaushik Tiwari – Department of Therapeutic Radiology, Yale School of Medicine, New Haven, Connecticut 06520, United States

Scott A. Strobel – Chemical Biology Institute and Department of Molecular Biophysics and Biochemistry, Yale University, West

Haven, Connecticut 06516, United States;  orcid.org/0000-0001-8402-4226

Complete contact information is available at:

<https://pubs.acs.org/10.1021/acs.jnatprod.0c00012>

Author Contributions

#N. Adaku and H. B. Park contributed equally to this work.

Notes

The authors declare no competing financial interest.

ACKNOWLEDGMENTS

This work was supported by grants from the Yale Comprehensive Cancer Center Swebilius Foundation to F.A.R., the National Institute of General Medical Sciences R01GM126211 to F.A.R., and the National Cancer Institute 1DP2-CA186575 to J.M.C. We thank Drs. Kaury Kucera and Michelle Legaspi Hutchings for their guidance on endophyte isolation and cultivation and Drs. Peter Glazer and Ranjit Bindra for providing cell lines. Endophytes were isolated from plants collected with permission of the Ministerio del Ambiente of Ecuador to S.A.S. and identified with the assistance of Percy Núñez Vargas.

REFERENCES

- (1) Ohgaki, H. *Methods Mol. Biol.* **2009**, *472*, 323–42.
- (2) Cancer Genome Atlas Research Network. *Nature* **2008**, *455* (7216), 1061–8.
- (3) Fruman, D. A.; Chiu, H.; Hopkins, B. D.; Bagrodia, S.; Cantley, L. C.; Abraham, R. T. *Cell* **2017**, *170* (4), 605–635.
- (4) Li, H. F.; Kim, J. S.; Waldman, T. *Radiat. Oncol.* **2009**, *4*, 43.
- (5) Jiang, Z.; Pore, N.; Cerniglia, G. J.; Mick, R.; Georgescu, M. M.; Bernhard, E. J.; Hahn, S. M.; Gupta, A. K.; Maity, A. *Cancer Res.* **2007**, *67* (9), 4467–73.
- (6) Yang, L. J.; Zhou, C. F.; Lin, Z. X. *Cancer Invest.* **2014**, *32* (2), 31–6.
- (7) Stupp, R.; Brada, M.; van den Bent, M. J.; Tonn, J. C.; Pentheroudakis, G.; Group, A. G. W. *Ann. Oncol.* **2014**, *25*, iii93–101.
- (8) Bastien, J. I.; McNeill, K. A.; Fine, H. A. *Cancer* **2015**, *121* (4), 502–16.
- (9) Torgovnick, A.; Schumacher, B. *Front. Genet.* **2015**, *6*, 157.
- (10) Hengel, S. R.; Spies, M. A.; Spies, M. *Cell Chem. Biol.* **2017**, *24* (9), 1101–1119.
- (11) Hartman, J. L. t.; Garvik, B.; Hartwell, L. *Science* **2001**, *291* (5506), 1001–4.
- (12) Bassi, C.; Ho, J.; Srikumar, T.; Dowling, R. J.; Gorrini, C.; Miller, S. J.; Mak, T. W.; Neel, B. G.; Raught, B.; Stambolic, V. *Science* **2013**, *341* (6144), 395–9.
- (13) Gupta, A.; Yang, Q.; Pandita, R. K.; Hunt, C. R.; Xiang, T.; Misri, S.; Zeng, S.; Pagan, J.; Jeffery, J.; Puc, J.; Kumar, R.; Feng, Z.; Powell, S. N.; Bhat, A.; Yaguchi, T.; Wadhwa, R.; Kaul, S. C.; Parsons, R.; Khanna, K. K.; Pandita, T. K. *Cell Cycle* **2009**, *8* (14), 2198–210.
- (14) Sulkowski, P. L.; Scanlon, S. E.; Oeck, S.; Glazer, P. M. *Mol. Cancer Res.* **2018**, *16* (8), 1241–1254.
- (15) Kang, Y. J.; Balter, B.; Csizmadia, E.; Haas, B.; Sharma, H.; Bronson, R.; Yan, C. T. *Nat. Commun.* **2017**, *8*, 14013.
- (16) McEllin, B.; Camacho, C. V.; Mukherjee, B.; Hahm, B.; Tomimatsu, N.; Bachoo, R. M.; Burma, S. *Cancer Res.* **2010**, *70* (13), 5457–64.
- (17) McCabe, N.; Hanna, C.; Walker, S. M.; Gonda, D.; Li, J.; Wikstrom, K.; Savage, K. I.; Butterworth, K. T.; Chen, C.; Harkin, D. P.; Prise, K. M.; Kennedy, R. D. *Cancer Res.* **2015**, *75* (11), 2159–65.
- (18) Mendes-Pereira, A. M.; Martin, S. A.; Brough, R.; McCarthy, A.; Taylor, J. R.; Kim, J. S.; Waldman, T.; Lord, C. J.; Ashworth, A. *EMBO Mol. Med.* **2009**, *1* (6–7), 315–22.
- (19) Mansour, W. Y.; Tennstedt, P.; Volquardsen, J.; Oing, C.; Kluth, M.; Hube-Magg, C.; Borgmann, K.; Simon, R.; Petersen, C.; Dikomey, E.; Rothkamm, K. *Sci. Rep.* **2018**, *8* (1), 3947.
- (20) Li, K.; Yan, H.; Guo, W.; Tang, M.; Zhao, X.; Tong, A.; Peng, Y.; Li, Q.; Yuan, Z. *Exp. Cell Res.* **2018**, *366* (1), 24–33.
- (21) Newman, D. J.; Cragg, G. M. *J. Nat. Prod.* **2016**, *79* (3), 629–61.
- (22) Bacon, C. W.; White, J. F. *Microbial Endophytes*; Marcel Dekker Inc: NY, 2000.
- (23) Rodriguez, R. J.; White, J. F., Jr.; Arnold, A. E.; Redman, R. S. *New Phytol.* **2009**, *182* (2), 314–30.
- (24) Hawksworth, D. L. *Mycol. Res.* **2001**, *105*, 1422–1432.
- (25) Strobel, G.; Daisy, B. *Microbiol. Mol. Biol. Rev.* **2003**, *67* (4), 491–502.
- (26) Tan, R. X.; Zou, W. X. *Nat. Prod. Rep.* **2001**, *18* (4), 448–59.
- (27) Wani, M. C.; Taylor, H. L.; Wall, M. E.; Coggon, P.; McPhail, A. T. *J. Am. Chem. Soc.* **1971**, *93* (9), 2325–7.
- (28) Gunther, E. *Ethnobotany of Western Washington*; University of Washington Press, 1945; Vol. 10.
- (29) Stierle, A.; Strobel, G.; Stierle, D. *Science* **1993**, *260* (5105), 214–6.
- (30) Stierle, A.; Strobel, G.; Stierle, D.; Grothaus, P.; Bignami, G. *J. Nat. Prod.* **1995**, *58* (9), 1315–24.
- (31) Wymann, M. P.; Bulgarelli-Leva, G.; Zvebil, M. J.; Pirola, L.; Vanhaesebroeck, B.; Waterfield, M. D.; Panayotou, G. *Mol. Cell. Biol.* **1996**, *16* (4), 1722–33.
- (32) Chernikova, S. B.; Wells, R. L.; Elkind, M. M. *Radiat. Res.* **1999**, *151* (2), 159–66.
- (33) Schultes, R. E.; Raffauf, R. F. *The Healing Forest: Medicinal and Toxic Plants of the Northwest Amazonia*; Dioscorides Press: Portland, OR, 1990.
- (34) Akgul, B.; Cooke, J. C.; Storey, A. J. *Pathol.* **2006**, *208* (2), 165–75.
- (35) Bass, M. S.; Finer, M.; Jenkins, C. N.; Kreft, H.; Cisneros-Heredia, D. F.; McCracken, S. F.; Pitman, N. C.; English, P. H.; Swing, K.; Villa, G.; Di Fiore, A.; Voigt, C. C.; Kunz, T. H. *PLoS One* **2010**, *5* (1), e8767.
- (36) Sancar, A.; Lindsey-Boltz, L. A.; Unsal-Kacmaz, K.; Linn, S. *Annu. Rev. Biochem.* **2004**, *73*, 39–85.
- (37) Nishigaki, R.; Watanabe, T.; Kajimoto, T.; Tada, A.; Takamura-Enya, T.; Enomoto, S.; Nukaya, H.; Terao, Y.; Muroyama, A.; Ozeki, M.; Node, M.; Hasei, T.; Totsuka, Y.; Wakabayashi, K. *Chem. Res. Toxicol.* **2009**, *22* (9), 1588–93.
- (38) Bontemps, N.; Bry, D.; Lopez-Legentil, S.; Simon-Levert, A.; Long, C.; Banaigs, B. *J. Nat. Prod.* **2010**, *73* (6), 1044–8.
- (39) Pearce, A. N.; Appleton, D. R.; Babcock, R. C.; Copp, B. R. *Tetrahedron Lett.* **2003**, *44* (20), 3897–3899.
- (40) Bindra, R. S.; Goglia, A. G.; Jasin, M.; Powell, S. N. *Nucleic Acids Res.* **2013**, *41* (11), e115.
- (41) Gunn, A.; Stark, J. M. *Methods Mol. Biol.* **2012**, *920*, 379–91.
- (42) Maity, A.; McKenna, W. G.; Muschel, R. J. *Radiother. Oncol.* **1994**, *31* (1), 1–13.
- (43) Hirai, T.; Shirai, H.; Fujimori, H.; Okayasu, R.; Sasai, K.; Masutani, M. *Cancer Sci.* **2012**, *103* (6), 1045–50.
- (44) Sun, J.; Wei, Q.; Zhou, Y.; Wang, J.; Liu, Q.; Xu, H. *BMC Syst. Biol.* **2017**, *11*, 87.
- (45) Hollander, M. C.; Blumenthal, G. M.; Dennis, P. A. *Nat. Rev. Cancer* **2011**, *11* (4), 289–301.
- (46) Bonfield, J. K.; Smith, K.; Staden, R. *Nucleic Acids Res.* **1995**, *23* (24), 4992–9.
- (47) Prakash, P. Y.; Irinyi, L.; Halliday, C.; Chen, S.; Robert, V.; Meyer, W. *J. Clin. Microbiol.* **2017**, *55* (4), 1011–1024.
- (48) Gonzalez, D.; Rodriguez-Carres, M.; Boekhout, T.; Stalpers, J.; Kuramae, E. E.; Nakatani, A. K.; Vilgalys, R.; Cubeta, M. A. *Fungal Biol.* **2016**, *120* (4), 603–619.
- (49) Paradis, E.; Claude, J.; Strimmer, K. *Bioinformatics* **2004**, *20* (2), 289–290.
- (50) Team, R. C. R v3.4.2; R Foundation for Statistical Computing: Vienna, Austria, 2017.

- (51) Team, R. *RStudio v1.1.383*; RStudio, Inc: Boston, MA, 2016.
- (52) Schliep, K. P. *Bioinformatics* **2011**, *27* (4), 592–3.
- (53) Stamatakis, A. *Bioinformatics* **2014**, *30* (9), 1312–3.
- (54) Yu, G. C.; Smith, D. K.; Zhu, H. C.; Guan, Y.; Lam, T. T. Y. *Methods in Ecology and Evolution* **2017**, *8* (1), 28–36.
- (55) Radu, A.; Neubauer, V.; Akagi, T.; Hanafusa, H.; Georgescu, M. *Mol. Cell. Biol.* **2003**, *23* (17), 6139–49.